Future Journal of
Pharmaceutical Sciences

RESEARCH

Open Access

QSAR, simulation techniques, and ADMET/pharmacokinetics assessment of a set of compounds that target MAO-B as anti-Alzheimer agent

Abduljelil Ajala[*], Adamu Uzairu, Gideon A. Shallangwa and Stephen E. Abechi

Abstract

Background: Alzheimer's disease (AD), the most common cause of dementia in the elderly, is a progressive neuro-degenerative disorder that gradually affects cognitive function and eventually causes death. Most approved drugs can only treat the disease alleviating the disease symptoms; therefore, there is a need to develop drugs that can treat this illness holistically. The medical community is searching for new drugs and new drug targets to cure this disease. In this study, QSAR, molecular docking evaluation, and ADMET/pharmacokinetics assessment were used as modeling methods to identify the compounds with outstanding physicochemical properties.

Results: The 37 MAO-B compounds were screened using the aforementioned methods and yielded a model with the following molecular properties: AATS1v, AATS3v, GATS4m, and GATS6e. Good statistical values were $R^2_{train} = 0.69$, $R^2_{adj} = 0.63$, $R^2_{pred} = 0.57$, $LOF = 0.23$, and $RMSE = 0.38$. The model was validated using an evaluation set that confirmed its robustness. The molecular docking was also utilized using crystal structure of human monoamine oxidase B in complex with chlorophenylchromone-carboxamide with ID code of 6FW0, and three compounds were identified with outstanding high binding affinity ($13 = -30.51$ kcal mol^{-1}, $31 = -31.85$ kcal mol^{-1}, and $33 = -33.70$ kcal mol^{-1}), and better than the Eldepryl (referenced) drug (-11.40 kcal mol^{-1}).

Conclusions: These three compounds (13, 31, and 33) were analyzed for ADMET/pharmacokinetics evaluation and found worthy of further analysis as promising drug candidates to cure AD and could also serve as a template to design several monoamine oxidase B inhibitors in the future to cure AD.

Keywords: Alzheimer disease, QSAR, Binding affinity, Pharmacokinetics, Molecular docking

Background

Alzheimer's disease (AD) is mainly identified by an extensive loss of neuronals in certain areas of the brain underlying a progressive decline in motor and cognitive functions [1, 2] and clinically characterized by deficiency of the important neurotransmitter acetylcholine (ACh), deposition of neurotoxic amyloid plaques (Aβ), highly phosphorylated tau proteins, and an imbalance in the glutamatergic system [3, 4]. Activated MAO induces the amyloid-beta (Aβ) deposition via abnormal cleavage of the amyloid precursor protein (APP), which contributes to the generation of neurofibrillary tangles and cognitive impairment due to neuronal loss as shown in Fig. 1 [5].

A few drugs are clinically approved for use which includes tacrine, galantamine, donepezil, and rivastigmine, which are cholinesterase inhibitors, whereas the fifth one memantine is a glutamatergic system modulator [6]. These drugs have limited efficacy and are associated with side effects such as hepatotoxicity [7]. The clinical

*Correspondence: abdulajala39@gmail.com
Department of Chemistry, Faculty of Physical Sciences, Ahmadu Bello University, P.M.B. 1044, Zaria, Kaduna State, Nigeria
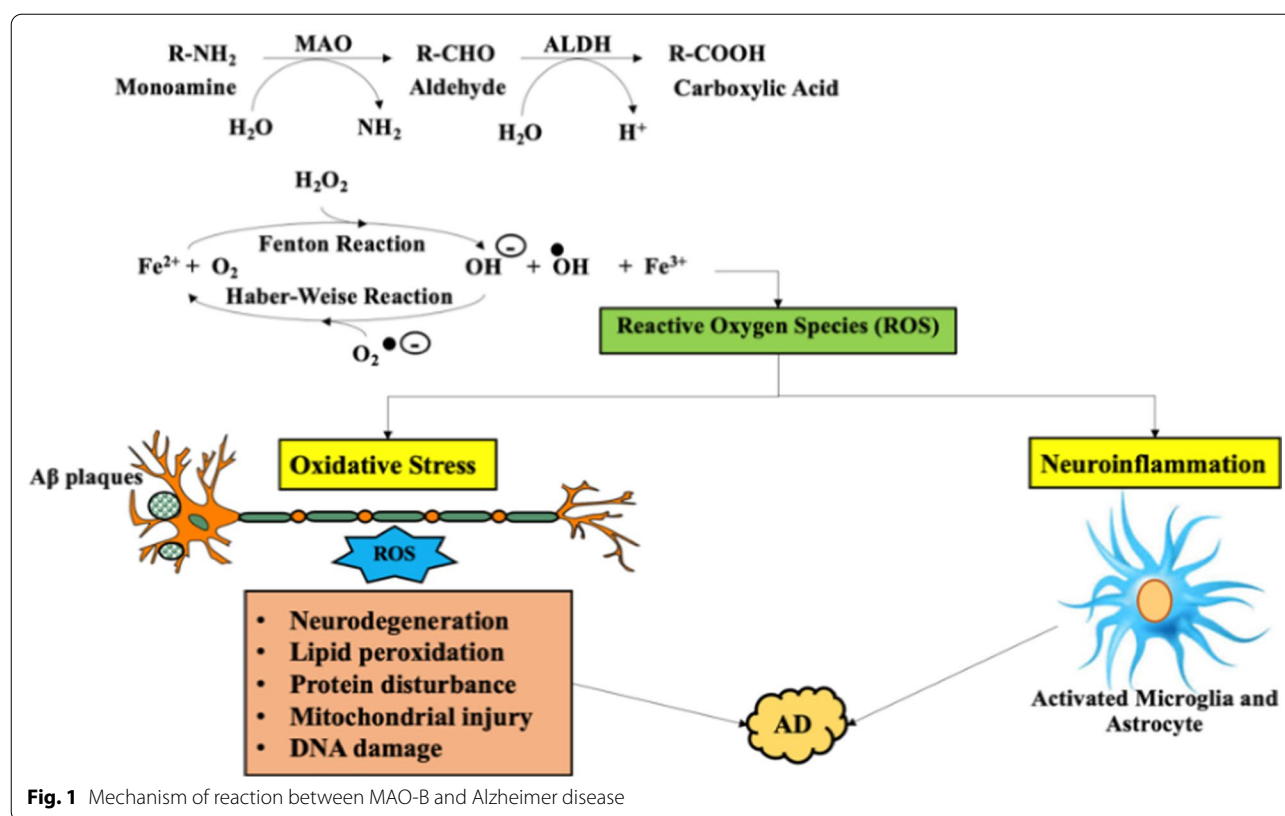
Fig. 1 Mechanism of reaction between MAO-B and Alzheimer disease

treatment of this disease is palliative and, in most cases, relies on improving stimulation at the relevant receptors by either increasing levels of the endogenous neurotransmitter [8] or by the use of substances that have a similar agonist response. Major advances in the treatment of AD include the use of acetylcholinesterase inhibitors such as galantamine, huperzine [9], and physostigmine and its derivatives to increase the levels of ACh rather than the use of cholinergic compounds, although compounds with nicotinic properties have attracted some interest [10]. Monoamine oxidase B (MAO-B) has recently emerged as a potential therapeutic target for AD because of its association with aberrant γ-aminobutyric acid (GABA) production in reactive astrocytes. The patients suffering from AD share a large plethora of pathogenic mechanisms and symptomatology [11]. To overcome such multifactorial diseases, an effective approach should consider molecules able to modulate different pathways. These scaffolds must be chosen among those recognized to interact pleiotropically with important and crucial systems such as MAO-B. To overcome this disease through a complex mechanism, computational studies of monoamine oxidase B inhibitors have the ability to cure or hinder the negative activity of AD [12].

Computational techniques include the use of quantitative structure–activity relationship (QSAR),

protein–ligand interaction (molecular docking), and drug kinetics studies and are major paths engaging in drug development and discovery processes [13]. Correlations between independent variables (experimental activities) and molecular properties (descriptors) of different classes of compounds are the backbone of QSAR [14], and the interactions between the molecules and ligands explain the molecular docking of the crystal structure of human monoamine oxidase B in complex with chlorophenylchromone-carboxamide with ID code 6FW0, while drug evaluation assessment explicates absorption, distribution, metabolism, excretion, and toxicity studies of a molecule that provides adequate information on properties that influence it [13]. Computer-assisted drug design (CADD) using the in silico techniques has been of significant importance in the identification and development of non-toxic, highly effective, and inexpensive drugs for the treatment or management of AD [13].

The principal aim of this study was to utilize QSAR, molecular docking, and drug evaluation assessment to determine the mechanism of interaction between promising compounds of MAO-B and protein target for the treatment of AD by analyzing their binding interactions through molecular docking, and to ADMET assessment in the human system.

Methods

Dataset

A total of thirty-seven datasets were taken from the literature [15] with the IC50 (µM) toward MAO-B inhibitors, and it was converted to PIC50 [16] with the aid of the expression $-\log(IC50/10^6)$, as presented in Table 1 with their molecular structures.

Virtual screening of dataset

Virtual screening (VS) is a powerful technique that has emerged as a reliable, cost-effective, and time-saving technique for the discovery and identifying hit molecules as starting points for medicinal chemistry [17].

Optimization and calculation of molecular property

ChemDraw Professional v 16.0 was used to draw the 2D molecular structures, which were saved in an SD file. Each of the molecules opened in Spartan'14, V 1.1.4, converting the 2D structures to 3D with the aid of tools in the Spartan software. Subsequently, density functional theory (DFT) (most probable structures and identification of the most stable conformer of the molecules associated with the absolute minima in the potential energy were achieved with the help of DFT) was carried out on the molecules utilizing Becke's three-parameter exchange functional hybrid with the Lee, Yang, and Parr correlation functional (B3LYP) and basis set of 6-31G** [18]. Molecular properties were extracted using the Spartan'14 package. In addition, the PaDEL descriptor software was used to generate molecular properties in addition to those from Spartan'14. Also, a total of 1500 molecular descriptors were calculated for the dataset as listed in Table 2.

Descriptors reception (treatment) and dataset division (training and evaluation set)

To generate a sturdy model with brilliant prediction, the intended molecular properties were ascertained. This is achieved with zero (0) and unwanted molecular properties [19]. Subsequently, the treated properties were divided into training and evaluation sets of 70 to 30 percent, respectively, utilizing Kennard and Stone's algorithm. The reason for the division is to use the training set to develop a QSAR model and the test set to evaluate the effectiveness of the developed model [20] (Table 3).

Descriptor selection, model building, quality, and model validation

QSARINS is a new software for the development and validation of MLR-QSAR models using the ordinary least squares method and genetic algorithm for variable selection [21]. This program mainly focuses on the external validation of QSAR models. This software was used to select the suitable descriptors. Thereafter, the foremost subset was selected using four descriptor combinations and an R^2 cutoff value of 0.6. The model quality was checked and validated using the Golbraikh and Tropsha acceptable model criteria such as $Q^2 > 0.5$, $R^2 > 0.6$, $R^2_{adj} > 0.6$, and $|r0^2 - r'0^2| < 0.3$ [22] (Table 4).

Descriptor importance and domain of applicability (DA)

The relative importance contribution of the descriptors was determined by the mean effect. Equation 1 defines the mean effect

$$NA_y = \frac{\beta_y \sum_{x=1}^{x=n} d_{xy}}{\sum_y^p \beta_y \sum_x^n d_{xy}} \tag{1}$$

where NA_y is the mean effect of descriptor y in a model, β_y is the coefficient of descriptor y in that model, d_{xy} is the value of the descriptor in the data matrix for each molecule in the training set, p is the number of descriptors that appear in the model, and n is the number of molecules in the training set. Thereafter, DA was assessed using the expression below to generate the hat matrix (leverages) to check for compounds that were outliers or influential with a threshold value of ± 3. This is expressed in Eq. 2

$$k_n = M_n \left(M^A M \right)^{-1} M_N^A \tag{2}$$

where K_n is the total number of descriptors values that made up the matrix *n*. Furthermore, Eq. 3 was used to screen molecules with variant leverage values to define the threshold limit for any controlling molecule [23].

$$k^* = 3\left(\frac{y+1}{q} \right) \tag{3}$$

Letter *y* represents the sum of descriptors in the model, while *q* represents number of molecules in the training data and k^* is the hat matrix (Table 5).

Y-randomization evaluation

Another standard validation evaluation parameter is Y-randomization, which measures the potency of the model. This assessment was established through rearrangement of the evaluation set [24, 25]. The molecular properties were constant to generate the model using multiple-linear regression while asserting the experimental activities. The products of Y-randomization are Q^2 and R^2, which must be low after about ten trials to confirm the robustness of the model and is clear evidence that the built model is of high quality and not, by the way, attained [26]. Furthermore,

Table 1 Molecular structures, activities, and docking scores

Compound		PIC50	ΔG (kcal mol^{-1})
1		0.95	− 21.76
2		1.94	− 28.03
3		0.67	− 23.91
4		0.45	− 28.26
5		1.18	− 27.10
6		1.71	− 25.73
7		2.38	− 23.24
8		1.71	− 24.81
9		0.99	− 27.78
10		1.96	− 23.82

Table 1 (continued)
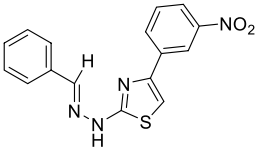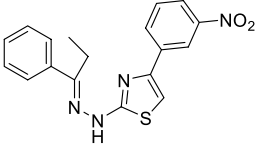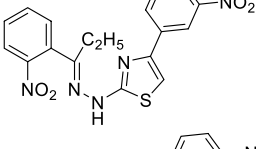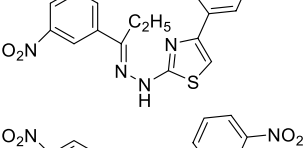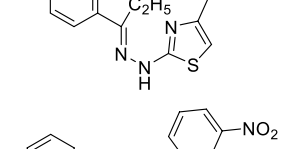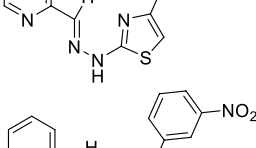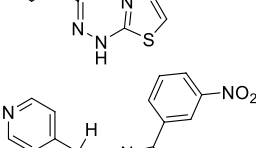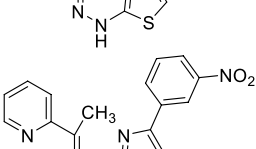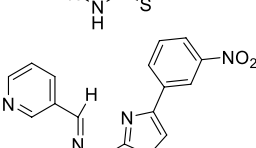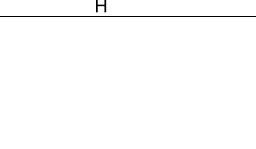
Compound		PIC50	ΔG (kcal mol^{-1})
11		1.69	− 25.53
12		1.81	− 23.61
13		2.19	− 30.51
14		2.04	− 25.25
15		2.27	− 23.86
16		1.98	− 28.04
17		1.45	− 26.84
18		2.57	− 20.81
19		1.70	− 24.61
20		1.69	− 24.75

Table 1 (continued)
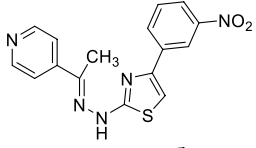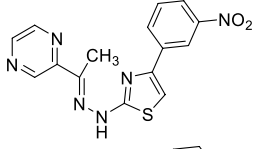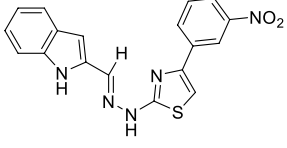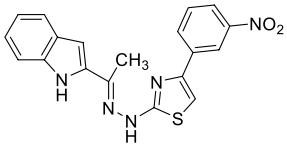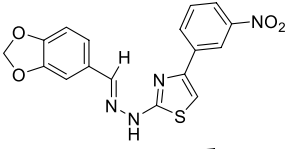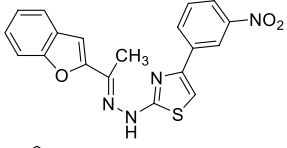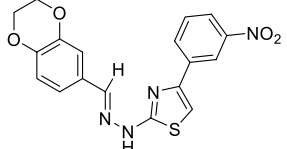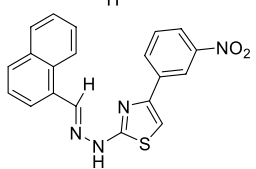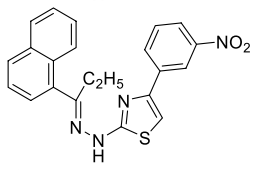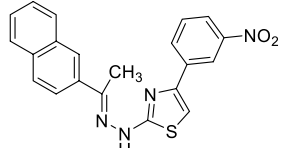
Compound		PIC50	ΔG (kcal mol^{-1})
21		1.37	− 25.63
22		2.09	− 28.66
23		1.76	− 25.02
24		2.46	− 25.33
25		2.36	− 23.92
26		2.37	− 13.97
27		0.68	− 25.06
28		2.00	− 28.02
29		1.56	− 23.95
30		1.87	− 20.46

Table 1 (continued)
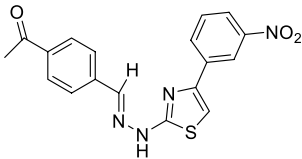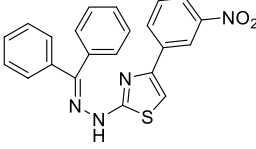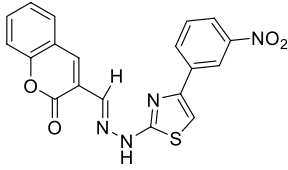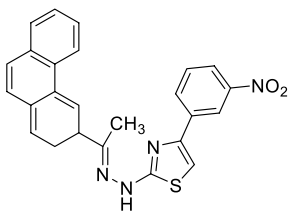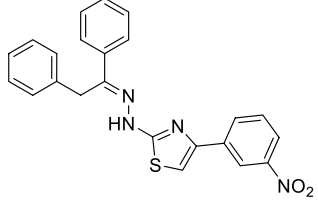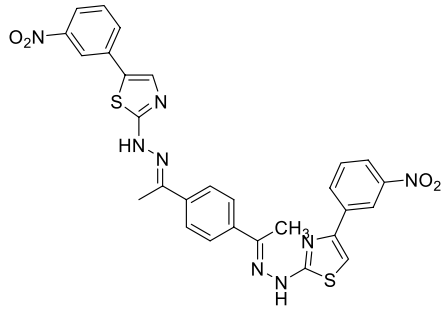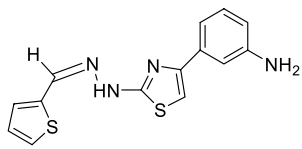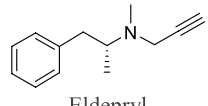
Compound		PIC50	ΔG (kcal mol^{-1})
31		1.67	− 31.85
32		0.22	− 24.38
33		0.81	− 33.70
34		1.97	− 23.92
35		1.37	− 16.54
36		1.59	− 20.85
37		1.11	− 20.83
Reference	Eldepryl		− 11.40

Table 2 Descriptor calculation for dataset

S/No	AATS1v	AATS3v	GATS4m	GATS6e	Observation	Predicted	Residual
Training set							
1	297.6475	218.9094	0.914028	0.994823	0.953276	1.580814	0.627537
2	299.4813	229.4111	1.006684	0.945055	1.943989	1.781762	0.162226
3	297.6913	217.562	0.898932	1.204206	0.674861	0.97591	0.301049
6	288.5722	219.0597	0.993292	0.854166	1.710963	2.229856	0.518893
8	297.0786	221.1226	0.934554	1.150817	1.705008	1.224355	0.480653
9	297.0786	222.8824	0.921167	1.175852	0.990339	1.383862	0.393523
10	297.0786	224.0321	0.926495	1.105338	1.963316	1.640273	0.323043
11	290.9698	221.9007	0.997955	1.070482	1.693727	1.606923	0.086804
12	291.1623	219.7585	1.005254	0.952702	1.812913	1.705119	0.107795
16	299.7762	223.0524	0.919195	1.069844	1.984077	1.482943	0.501134
17	294.302	223.5601	0.992318	1.083972	1.448706	1.456079	0.007373
18	298.1829	231.6285	0.981774	0.860283	2.569374	2.477758	0.091616
19	298.1832	227.91	1.030283	0.991369	1.696356	1.481619	0.214737
23	309.4127	224.234	0.750577	1.158026	1.755875	1.643182	0.112693
24	298.1836	230.4134	0.979708	1.087878	2.456366	1.747631	0.708735
25	295.0909	225.815	0.96714	0.9321	2.356026	2.170345	0.185681
26	300.7947	223.0978	0.880166	0.945471	2.372912	2.016283	0.356629
27	306.8214	236.7577	0.994401	1.280024	0.683047	0.875783	0.192736
28	296.2707	225.4369	0.955922	0.914134	2.004321	2.166517	0.162196
29	309.5633	206.3861	0.612291	1.033981	1.559907	1.488068	0.071838
30	295.6709	235.1477	1.077964	1.027411	1.868644	1.849744	0.018901
32	301.9736	226.8351	1.09348	1.119595	0.220108	0.284052	0.063944
33	295.6503	213.7543	1.019817	0.926949	0.810904	0.819565	0.008661
34	319.6262	237.6001	0.77405	0.986436	1.974512	2.173184	0.198672
36	299.4813	231.4712	0.947273	1.041653	1.593286	2.071609	0.478323
37	299.4813	229.4111	0.965993	1.113519	1.107211	1.576788	0.469577
Test set							
4	286.5247	208.8337	0.958307	0.924432	0.451786	1.622659	1.170872
5	288.5722	220.7687	0.944413	1.112229	1.184691	1.961825	0.777134
7	288.5722	219.0597	1.02677	0.698291	2.382017	2.447592	0.065575
13	297.0786	222.8824	0.921167	1.175852	2.193125	1.383862	0.809262
14	290.9698	225.6169	0.985946	1.136569	2.037426	1.796752	0.240675
15	290.2124	227.6915	1.001267	1.099253	2.274158	2.029735	0.244423
20	292.6929	219.4861	0.96768	0.769254	1.687529	2.327697	0.640168
21	303.6736	232.168	0.919552	1.157647	1.372912	1.628114	0.255202
22	293.3524	222.7396	0.944523	0.925934	2.089905	2.242083	0.152178
31	301.0308	211.4888	0.657551	1.459484	1.671173	1.106193	0.56498
35	297.6913	217.562	0.898932	1.204206	1.369216	0.97591	0.393306

c$R2p \geq 0.5$ for the Y-randomization coefficient must be satisfied to ascertain the goodness of the model [27]. Equation 4 was used to compute the Y-randomization coefficient.

$$cR_p^2 = R \times i\left[R^2 - R_r^2\right]^{2i} \tag{4}$$

Preparation of protein target and ligand

The human crystal structure of monoamine oxidase B (MAO-B) in complex with chlorophenylchromone-carboxamide (PDB ID: 6FW0; chain B) was retrieved from RCSB PDB database (https://www.rcsb.org/), and

Table 3 Molecular properties utilized in the MLR model

S/No	Identity of molecular properties	Descriptor sign	Class	% Contribution
1	An averaged Moreau-Broto autocorrelation of lag 1 weighted by vdw volume	AATS1v	2D	48%, and negative contribution (0.08492)
2	An averaged Moreau-Broto autocorrelation of lag 3 weighted by vdw volume	AATS3v	2D	34%, and positive contribution (0.07988)
3	A Geary autocorrelation coefficient lag1 which is weighted by atomic mass	GATS4m	2D	12%, and negative contribution (6.73046)
4	Geary autocorrelation—lag 6/weighted by atomic Sanderson electronegativities	GATS6e	2D	6%, and negative contribution (2.84241)

Table 4 Y-randomization assessment of MLR

Model type	R	R^2	Q^2 (LOO)
Original	0.827819	0.685284	0.574515
Random 1	0.412459	0.170122	− 0.48832
Random 2	0.47985	0.230256	− 0.51132
Random 3	0.255063	0.065057	− 0.741
Random 4	0.279267	0.07799	− 0.35473
Random 5	0.411131	0.169028	− 0.69774
Random 6	0.366618	0.134409	− 0.27287
Random 7	0.422091	0.178161	− 0.34895
Random 8	0.484999	0.235224	− 0.18176
Random 9	0.515376	0.265613	− 0.03472
Random 10	0.348056	0.121143	− 0.29197
Average R	0.436612		
Average R^2	0.212026		
Average Q^2 (LOO)	− 0.30444		
cRp^2	0.601116		

it was treated for the removal of water molecules and heteroatoms. The protein possesses the following characteristics which makes it useable, low resolution of 1.60 Å, Homo sapiens, no mutation and has been establish in the literature. Further, the inhibitor binding site of co-crystal ligand/inhibitor was untangled from the literature available for the crystal structure [28]. Size of the grid box 40 Å × 40 Å × 40 Å was built that engulfs the inhibitor binding pocket for the protein structure at the coordinates $x = 50.514803$ Å, $y = 155.997795$ Å, and $z = 29.023735$ Å. On the other hand, the two-dimensional molecular structures of the chemical compounds were drawn and their 3D structures were optimized using Spartan'14. Further, the ligand preparation for docking was carried out in Discovery Studio as described in a previous research by [29, 30] (Table 6).

Molecular docking procedures and docking validation protocols

The ligands were virtual screened using the Internal Coordinate Mechanics Program (ICM-PRO). The ICM

Table 6 Virtual screening of the compounds docked against the target protein

Compound	Binding affinity (kcal mol^{-1})	Total no. of intermolecular bonds	Total no. of hydrogen bonds
13	− 30.51	8	2
31	− 31.85	9	1
33	− 33.70	19	9
Eldepryl (Reference)	− 11.40	3	1

Table 5 Correlation and statistical evaluation assessment of the selected molecular properties

	AATS1v	AATS3v	GATS4m	GATS6e	VIF	P value	MEAN EFFECT	Class	% Contribution of each descriptor
AATS1v	1				0.8579	0.0030	1.5178	2D	48
AATS3v	0.3423	1			0.7843	0.0009	− 1.0742	2D	34
GATS4m	− 0.5735	0.3841	1		0.4370	0.0001	0.3797	2D	12
GATS6e	0.3282	0.0394	− 0.3722	1	0.8683	0.0001	0.1766	2D	6

scoring algorithm employs Monte Carlo simulations to optimize ligand internal coordinates in the space of grid potential maps produced for the protein pocket and weighted as follows [31]. To screen the 3D conformations of chemical compounds derived via docking, the binding affinity with intermolecular connections and hydrogen bonds with the target protein was employed. Based on these criteria, a possible inhibitor chemical with the highest binding affinity and number of contacts was identified. The introduction of a random move to one of the rotational, translational, or conformational within the binding pockets of the variables; minimization energy of the differentiable terms; calculation of desolvation energy; and the final minimized conformation is accepted or rejected based on Metropolis criterion [30, 31], and the maximal number of steps is achieved after repetition of the procedure. The predicted score is calculated by following Eq. 5. Reliability and worthiness ability of the docking method were validated with the aid of glide module in Schrodinger, version 18.0 suite.

$$\Delta G = \Delta E_{\text{IntFF}} + T\Delta S_{\text{Tor}} + \alpha_1 \Delta E_{\text{HBond}}$$
$$+ \alpha_2 \Delta E_{\text{HBDesol}} + \alpha_3 \Delta E_{\text{SolEI}} \quad (5)$$
$$+ \alpha_4 \Delta E_{\text{HPhob}} + \alpha_5 Q_{\text{size}}$$

where ΔE = energy change, IntFF = internal force field, HBond = hydrogen bond, HBDesol = hydrogen bond donor–acceptor desolvation, SolEI = solvation electrostatic energy ligand binding, HPhob = hydrophobic free energy gain, and size correction term.

In silico prediction of ADME, pharmacokinetics, and bioactive evaluation

The chemoinformatic technique is one of the current and agile growing and becoming elaborate approaches in pharmacokinetics, ADME (absorption, distribution, metabolism, excretion) assessment, drug discovery, and toxicity. Various pharmacokinetic (PK) parameters can now be forecasted via quantitative in silico method [32]. The strong consensus is that the forecasts are no worse than those obtained by in vitro experiments, with the significant advantage of requiring far less technology, resources, and time. In addition, and of critical importance, it is possible to screen virtual compounds. The predictions were executed utilizing SwissADME web tool, pkCSM, and molinspiration. Bioactive and medicinal chemistry evaluation of the compounds was investigated using web-based online tools [33] (Table 7).

Results

QSAR results evaluation

QSAR-MLR approach was effect-fully computed on derivatives of monoamine oxidase B as potential inhibitors against AD.

Character of descriptors in the model
Built model

$$PIC50 = 18.35217(+/-5.55493)$$
$$- 0.08492(+/-0.02234)\textbf{AATS1v}$$
$$+ 0.07988(+/-0.01636)\textbf{AATS3v} - 6.73046$$
$$(+/-1.43217)\textbf{GATS4m} - 2.84241$$
$$(+/-0.71084)\textbf{GATS6e}$$
$$(6)$$

N_{train}: 26, N_{test}: 11, R^2: 0.6853, R^2_{adj}:0.6253, LOF: 0.2274, Q^2_{loo}: 0.5745, RMSE cv: 0.3839, PRESS cv: 3.8310, CCC cv: 0.7510, RMSE ext: 0.2818, MAE ext: 0.1831, PRESS ext: 0.2237.

Analysis and receptor plot

Figure 6 shows predicted protein target plot of Ramachandran, and the quality of the plot was ascertained by online software.

Molecular docking (MD) procedures and docking validation protocols

All the compounds, including the reference compound, were subjected to MD procedures, but only a few of them had higher binding scores than 30 kcal mol^{-1}, such as compounds 13, 31, and 33, which had higher binding affinities of − 30.51, − 31.85, and − 33.70 kcal mol^{-1}, respectively, and were chosen for further analysis.

In silico prediction of ADMET, pharmacokinetics, and bioactive evaluation

Table 8 shows the physicochemical parameters of docked compounds based on their binding affinity, and the best-docked molecules are evaluated as potential drug candidates (Table 9).

Table 10 displays the predicted bioactivity scores as well as the medicinal chemistry characteristics of numerous developed drugs [34]. The G protein-coupled receptor (GPCR) ligand, ion channel modulator, nuclear receptor ligand, kinase inhibitor, and enzyme inhibitor were all given bioactivity scores for the compounds that were chosen. The molecule is deemed more bioactive if

Table 7 Detailed binding interactions of compounds with the protein with distances in (Å)

Compounds	Hydrogen bonds	Hydrophobic bonds				Electrostatic bonds	Others
		π–π	π-Alkyl	Alkyl	π-Sigma	π-Anion	π-Sulfur
13	ASN 116 (3.35), ARG 127 (3.16)	PHE 103 (5.11)	TYR 112 (5.19), ARG 120 (3.77), ARG 484 (5.38)	–	THR 479 (3.35)	GLU 483 (4.03)	–
31	TYR 435 (3.37),	TYR 326 (5.30)	TYR 398 (5.31), TYR 398 (3.74)	LEU 171 (4.92)	LEU 171 (3.37), ILE 199 (3.58)	–	CYS 172 (5.45), PHE 343 (5.70)
33	SER 59 (3.47), TYR 60 (3.47), CYS 172 (3.67), CYS 397 (2.93), TYR 435 (3.07), CYS 172 (3.27), CYS 172 (3.26), GLY 434 (3.51), TYR 435 (3.12)	TRP 388 (5.12), GLY 57 (3.58), GLY 57 (4.03)	PHE 343 (5.44), TYR 398 (5.39) LYS 296 (4.94) CYS 397 (4.39) CYS 397 (4.34)	LEU 171 (5.41)	–	–	TYR 60 (4.98)
Eldepryl (Reference)	GLN 206 (3.14)	–	TYR 398 (5.45), TYR 435 (4.21)	–	–	–	–

Table 8 Predicted physicochemical parameters of MAO-B inhibitor and referenced drug

Parameters	Compounds			
	13	31	33	Reference
Molecular weight < 500	397.41	366.39	392.39	273
nHBA < 10	6	5	6	4
nHBD < 5	1	1	1	1
nROTB < 9	7	6	5	1
Log P < 5	2.71	3.02	3.13	5.1
TPSA < 130	107.16	128.41	115.56	30.5
GI absorption	High	High	High	Low
BBB permeation	No	No	No	No
PAINS alerts	0	0	0	1
Lipinski's rule violation	0	0	0	1
Bioavailability score	0.55	0.55	0.55	0.55

Table 9 Predicted ADME properties of designed inhibitors

Compounds	13	31	33	Reference
GIA (% Absorbed)	97.47	97.50	100	81.51
LogK$_P$ (skin permeation)	− 5.24	− 5.43	− 5.64	− 2.5
P-gp S	Yes	Yes	Yes	No
CaCo$_2$ (log Papp in 10–6 cm/s)	1.16	1.11	1.16	0.11
CYP 3A4	No	Yes	Yes	No
CYP 2D6	No	No	No	Yes
Hepatotoxicity	No	No	No	No

the expected value is greater than 0.00 (> 0), moderately active if the value is between 0.5 and 0.00, and non-active if the expected value is less than 0.5. As demonstrated in Table 10, all of the substances tested, with the exception of the Eldepryl which is the referred drug, are active G protein-coupled receptor (GPCR) ligands with projected bioactive values greater than 0.00. It was also looked into PAINS alerts (pan assay interference) and synthetic accessibility for medicinal chemistry properties. There was no alarm in any of the considered compounds, except the referenced medications (PAINS alert = 0). A synthetic accessibility or complexity score of 1–4 indicates that synthesis is simple, 4–7 indicates that it is moderate, and 8–10 indicates that it is challenging inhibitors [35]. In addition, Fig. 11 shows the BOILED-egg to ascertain the permeability of the active compounds in the BBB (blood–brain barrier) or HIA (human gastrointestinal (HIA) absorption). All the studied compounds and the standard drug had a favorable physiochemical profile because their expected values were within the limit.
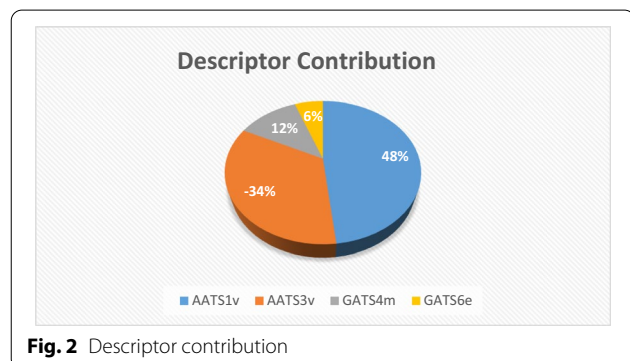
Discussion
QSAR results evaluation
The developed QSAR model established in this study was utilized for the prognostic of anti-Alzheimer activities with the influence of the calculated molecular properties. The calculated properties are AATS1v, AATS3v, GATS4m, and GATS6e which made up the MLR model supply a significant influence in revamping the chemical information of each compound into numeral value as

Table 10 Bioactivity index and medicinal chemistry accessibility of designed inhibitors

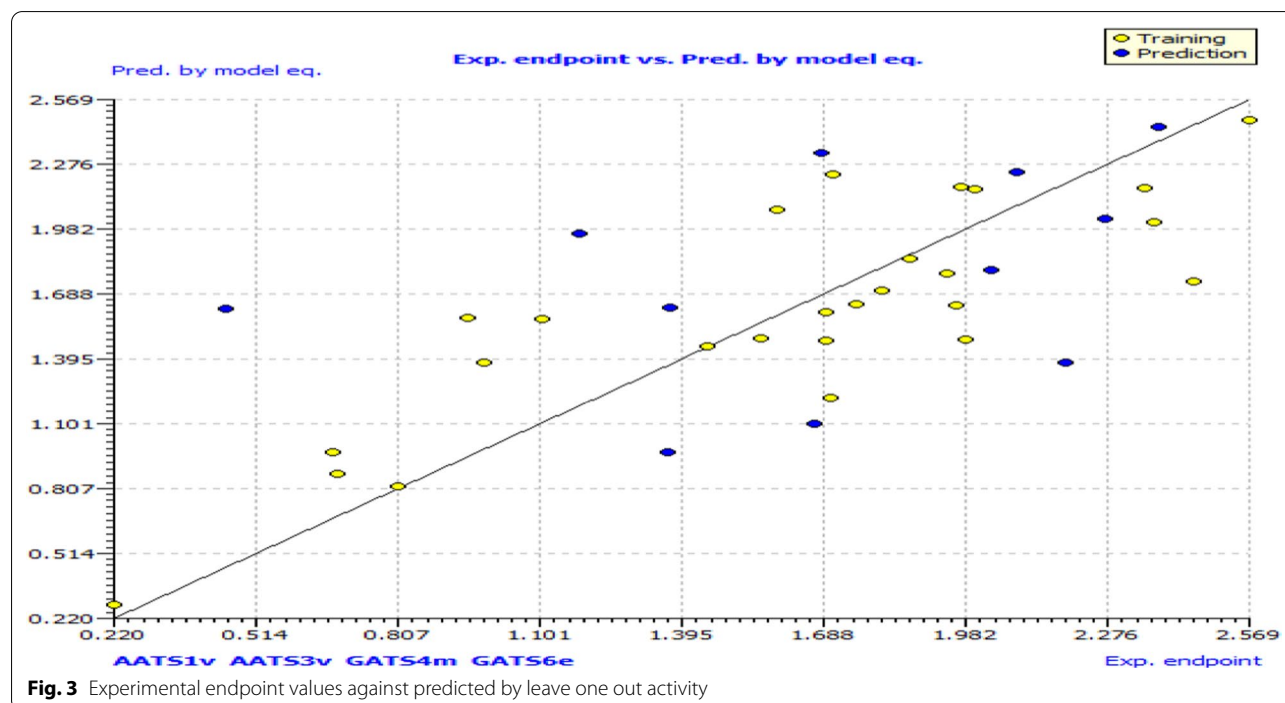| Compounds	GPCR	1CM	KI	NRL	PI	EI	SA	GV	VV	EV	MV	PA
13	0.59	− 0.55	− 0.64	− 0.72	− 0.55	− 0.30	3.56	0	0	0	0	0
31	0.70	− 0.84	− 0.62	− 1.07	− 0.76	− 0.38	3.25	0	0	0	0	0
33	0.74	− 0.94	− 0.61	− 0.92	− 0.64	− 0.26	3.62	0	0	0	0	0
Eldepryl	− 0.56	− 0.11	− 0.24	− 0.48	− 0.50	− 0.31	5.12	1	0	1	0	1

GPCR G protein-coupled receptor, *ICM* ion channel modulator, *KI* kinase inhibitor, *NRL* nuclear receptor ligand, *PI* protease Inhibitor, *EI* enzyme inhibitor, *SA* synthetic accessibility, *GV* Ghose violation, *VV* Veber violation, *EV* Egan violation, *PA* pain alert, *MV* Muegge violation

Fig. 2 Descriptor contribution

Character of descriptors in the model

Table 3 shows the technical meaning of each descriptor as featured in the built model. The physicochemical interpretation of the above QSAR model is denoted by the contribution of modeled parameters including an averaged Moreau-Broto autocorrelation of lag 3 weighted by vdw volume (AATS3v) with maximum positive impact, whereas decrease in values of parameters such as an averaged Moreau-Broto autocorrelation of lag 1 weighted by vdw volume (AATS1v), a Geary autocorrelation coefficient lag1 which is weighted by atomic mass (GATS4m), and Geary autocorrelation—lag 6/weighted by atomic Sanderson electronegativities (GATS6e), may increase activities of the receptor. These descriptors contribute aromaticity, hydrophobicity, and hydrogen bonding responsible for increase in the ligand affinity to bind to the protein target [38, 39].
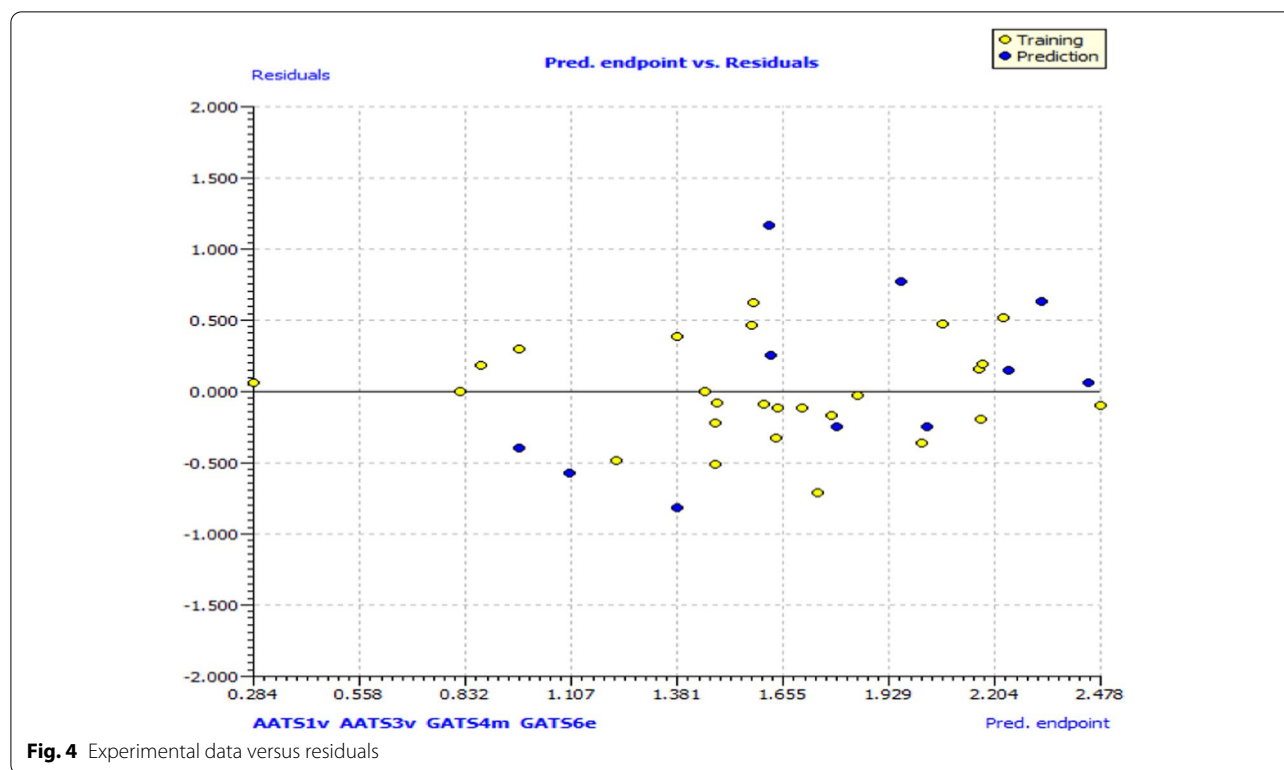
reported in Table 2. Also, in Table 2, the predicted activities with the help of the calculated molecular properties as well as the residual values for all the studied compounds are presented.

Fig. 3 Experimental endpoint values against predicted by leave one out activity

Fig. 4 Experimental data versus residuals

The low value computed for the residual between predicted and observe activities gives a reasonable suggestion that the model has a reliable predictive measure [40]. For the moment, the built QSAR model was strongly derived utilizing the approach of QSAR-MLR with four dynamic molecular properties integrated into the equation as shown below.

The model as the following values as it internal parameters for its indestructibility and consistently well ability, R^2 (correlation coefficient) of 0.6853, R^2_{adj} (adjusted correlation coefficient) of 0.6253, and Q^2_{loo} (leave one out cross-validation correlation coefficient) of 0.5745 in order to confirm its efficacy for predicting the activities of the studied inhibitors. More also, Table 4 shows MLR Y-randomization test, the strength, and consistent of the built model were verified by the coefficient of Y-randomization of 0.6433 shown in Table 4. Interestingly, it was observed that all the validation criteria were fully agreed with the acceptable threshold parameters stated in a literature [36].

Accuracy and cogency of the selected properties were commutated through correlation assessment with other statistical quantities. The parameters reported in Table 5 fall within the limit value of < 10 for variance inflated factor (VIF) which implies that each descriptor is orthogonal to one another and in agreement with the Pearson correlation analysis to ascertain the estimated results [37]. Also, the correlation coefficient of ≤ 0.8 indicates that the properties were parallel to each other and no multicollinearity within the descriptors [38].

Table 5 shows the scalar and vector ability of the molecular properties estimated through mean effect (ME) evaluation. It is observed from results shown in Table 5 that descriptor AATS1v has the highest ME value of 1.5178. Figure 2 shows the percentage contribution of all the descriptors, and the first descriptor AATS1v is 48% with highest percentage contribution to the developed model and increases the activity of the model in a positive direction. The ME value of the second descriptor AATS3v is -1.0742 with percentage contribution of 34% with the second highest percentage contribution to the built model and increases the activity of the model in a positive direction. Also, the third descriptor *GATS4m* with a ME value of 0.3797 and 12% contribution to the model influences the activity of the model in a positive direction. Lastly, the descriptor GATS6e with a ME value of 0.1766 and 6% contribution to the developed model influences the model in a positive direction. Still in Table 5, it shows the variance analysis between the computed properties and their activities (called p values). All the values were found to have $p < 0.05$ at ninety-five percent confidence limit. Hence, alternative hypothesis is valid and acceptable [40].

Fig. 5 Williams plot

Fig. 6 Ramachandran graph. Most favored region (red), additional allowed region (brown). Generously allowed region (deep yellow)
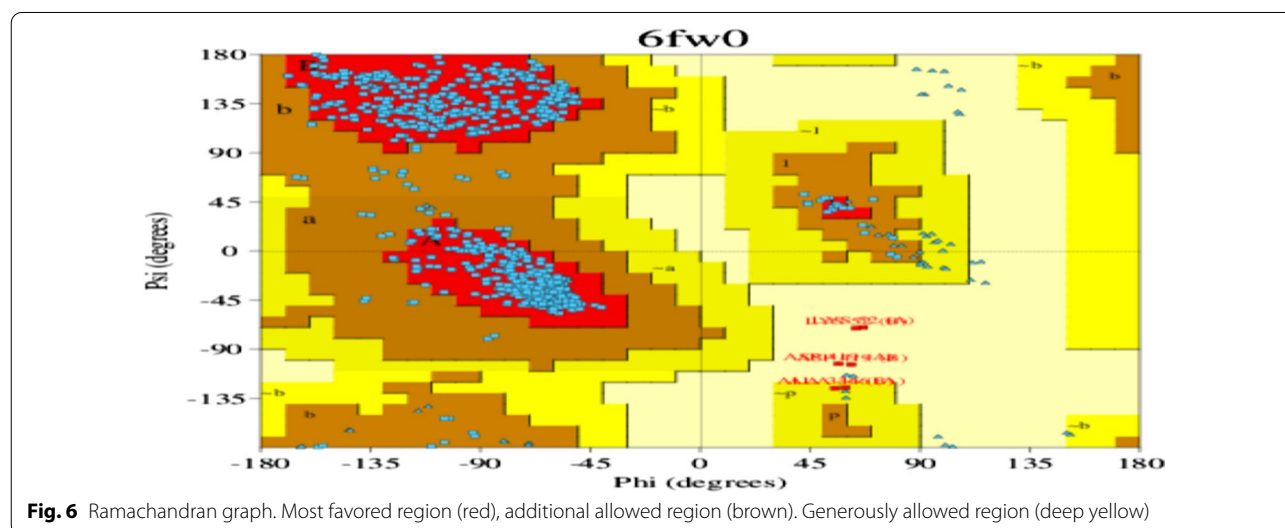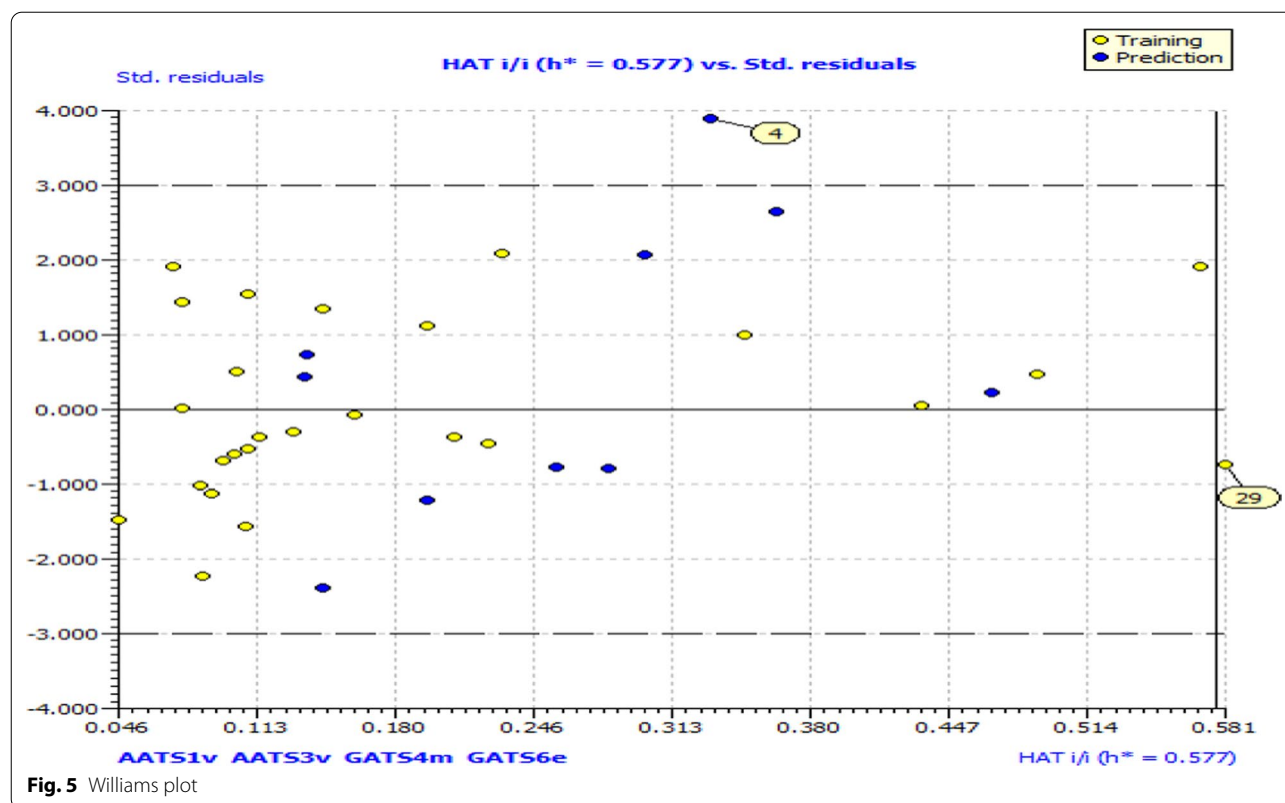
Figure 3 shows a scatter plot of the experimental versus the predicted responses. This enables the detection of systematic trends and clustering of data and, if any, sturdy outliers in the data. In this plot, there are neither systematic trends nor clustering of data, and this simply indicates strength of the developed model and its reliability [41].

Figure 4 indicates the plot of experimental against residuals. This plot gives room to evaluate the deviations from the ideal experimental and predicted value and to detect anomalous trends. The plot shows equal distribution of the data within $+2$ and -2, hence no anomalous detected which implies that the built model is brilliant and offer exceptional predictions [42].
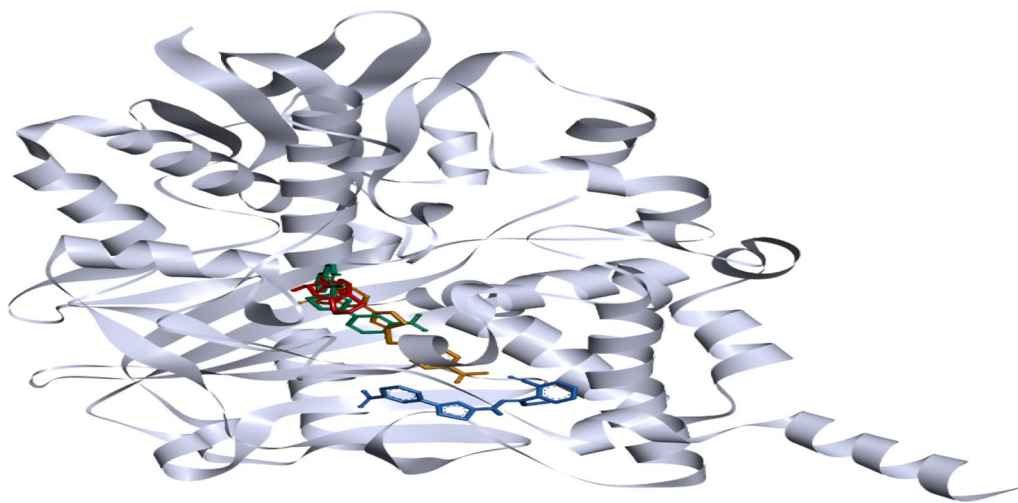
Fig. 7 Binding of the compounds inside the inhibitor binding site of the protein. Blue: compound 13, orange: compound 31, green: compound 33, and red: reference

Figure 5 shows the Williams plot called DA for the detection of outliers for the response (dependent variables) and those for the structure (independent variables). It consists of plotting the standardized residuals on the *y*-axis and the leverage values from the hat matrix diagonal on the *x*-axis [43]. All the chemical compounds (obviously from Fig. 3) fall within the domain of ± 3 with the exception of compound 4 which falls above the user defined threshold, thus considered as outliers. Also, only compound 39 is observed to overshoot the danger zone called "warning leverage" ($h*$) of 0.58. Thus, an influential hypothetical compound with magnified activities which cannot be taken into consideration when designing theoretical compounds.

Analysis and receptor plot

The Ramachandran plot demonstrated an appropriate percentage distribution of protein residues, indicating that the predicted model was of sufficient quality to match the protein stereochemistry in the final model [44]. Also, the plot provides away to view the distribution of torsion angles in a protein structures as shown in Fig. 6 called Ramachandran graph.
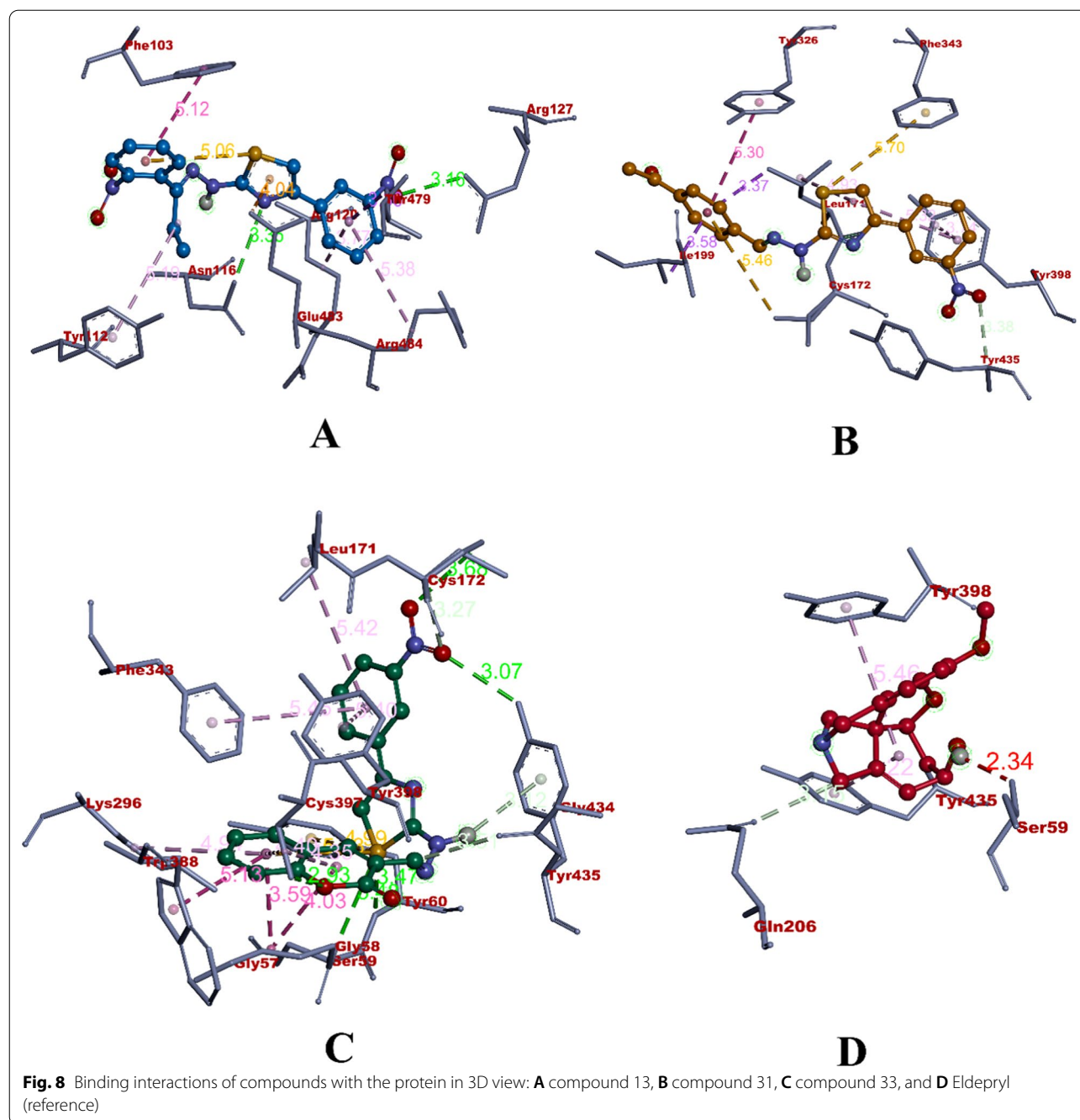
Molecular docking (MD) procedures validation protocols

All the compounds except 13 occupied the central inhibitor binding site, which is located near to the flavin adenine dinucleotide (FAD) binding region. Compound 13 chiefly occupied the loop region which is present between 99 and 105 residues as shown in Fig. 7. All the compounds were found to bind the co-crystal inhibitor ligand (E92602). Among all the compounds, compound 33 was found to have the highly negative, binding affinity ($- 33.70$ kcal mol^{-1}) with hydrogen and hydrophobic interactions, whereas the Eldepryl (reference) was found with the lowest binding affinity ($- 11.40$ kcal mol^{-1}). The details of virtual screening are depicted in Table 6.

According to the [28], the binding of the compounds within the inhibitor binding site/active site of the protein would allow the molecule to interact with the key residues like TYR 435, CYS 397, CYS 172, PHE 343, TYR 398, and LYS 296 [47]. However, compound 13 was not able to get inserted in the binding pocket. In case of reference, although it got inserted in the binding pocket, the number of interactions and binding affinity were comparatively low. Binding interactions of the compounds with the amino acid residues of the target protein are detailed in Table 7. Also, the visualization of these interactions is given in Fig. 8 (3D) and Fig. 9 (2D). The docking and binding of the compounds were accurate according to, where natural phenols were evaluated to inhibit the binding site of the human MAO using both in vitro and in silico approaches (PDB ID: 6FW0). In similar study conducted by Catalano et al. [48], 1 H-pyrrolo-[3, 2-c] quinolines were evaluated against the human MAO using in vitro and in silico methods. With the compounds showing similar binding pattern in term of binding energy (inhibitor binding site located near to the FAD region) and interactions (both hydrogen and hydrophobic interactions with the key residues), as previously reported [49]. By the virtue of these interactions, as mentioned in [48], inhibition of human MAO could be achieved by our compounds.

Figure 10 shows the superimposed structures of the docked and co-crystalline ligands with RMSD value of

Fig. 8 Binding interactions of compounds with the protein in 3D view: **A** compound 13, **B** compound 31, **C** compound 33, and **D** Eldepryl (reference)

1.7453 Å which is less than threshold value of ±2. This is a clear evidence that validation of our docking method was good and yielded excellent result.

In silico prediction of ADMET, pharmacokinetics, and bioactive evaluation

However, when utilizing appropriate processes in drug design, development, and discovery expeditions, it is essential to evaluate some critical pharmacokinetic characteristics or ADMET properties (absorption, distribution, metabolism, excretion, and toxicity) as the most vital characteristics [36]. Lipinski's rule of five was used to analyze the expected properties that play a significant role in a molecule's efficacy, safety, or metabolism for all of the docked compounds. The results revealed that none of the compounds, with the exception of the referenced medication (Eldepryl), have Lipinski's rule of five violations (RO5) violated.
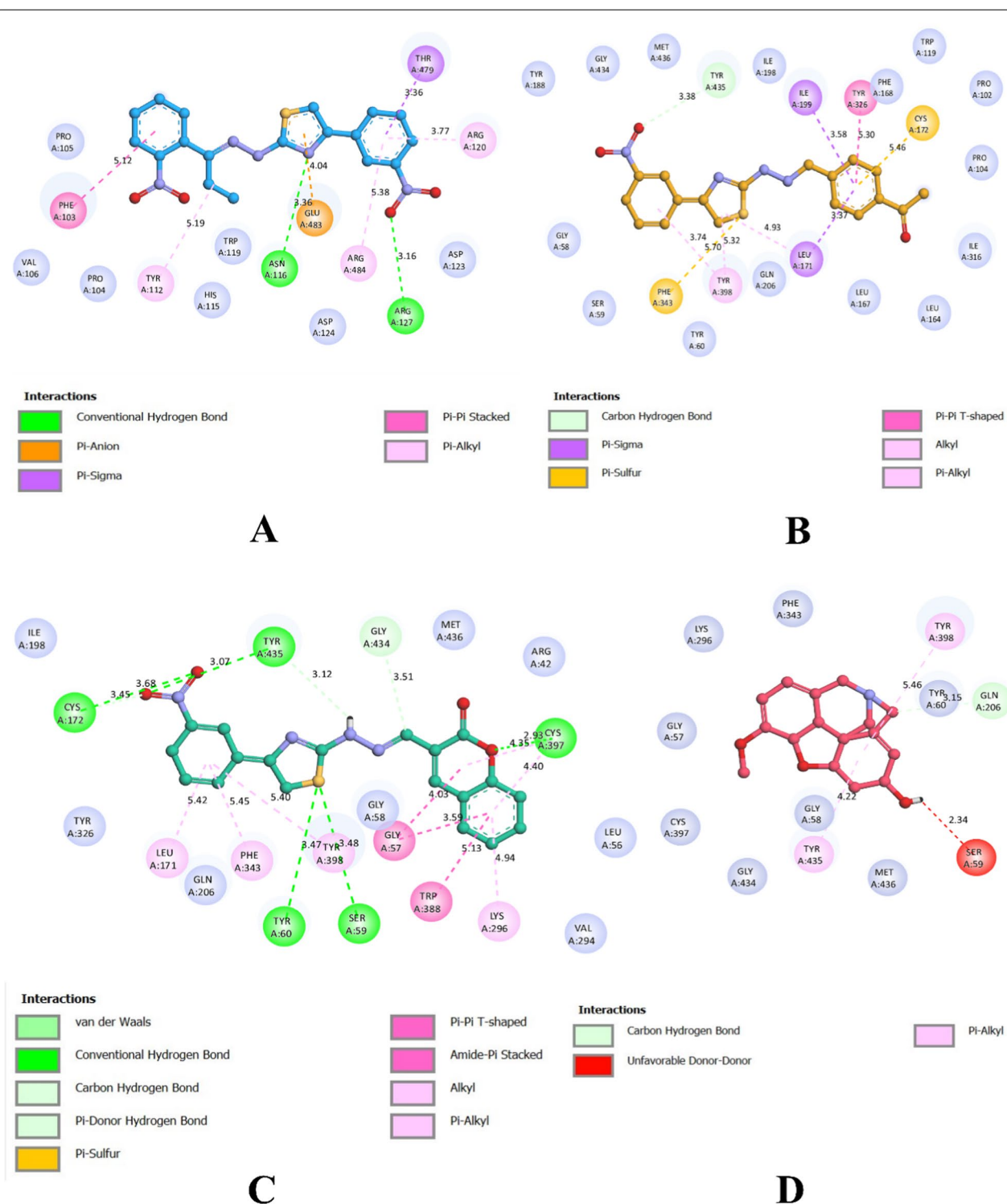
Fig. 9 Binding interactions of compounds with the protein in 2D view: **A** compound 13, **B** compound 31, **C** compound 33, and **D** Eldepryl (reference). Lavender: surrounding residues, colored: binding residues
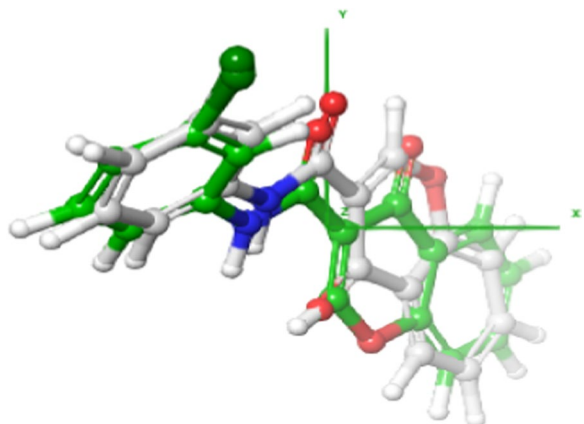
Fig. 10 RMSD value of 1.7453 Å for superposition of the co-crystal ligand with its docked pose

This demonstrates that all the three inhibitors have drug-like or pharmacological qualities, allowing them to be taken orally. Table 9 shows ADMET qualities of the three compounds thoroughly investigated using online web-based tools, and the results were compared to a referred drug (Eldepryl), Based on ADMET predictions, the computed absorption properties (percent human intestinal absorption > 30%, Caco2 permeability > 0.90, and skin permeability $\log Kp > 2.5$) were found to be within the threshold values, and all of the selected compounds, with the exception of the referenced drug, were found to be P-glycoprotein II inhibitors. This suggests that all of the compounds had significant pharmacological properties and were well absorbed by humans [50]. Similarly, Fig. 11 shows the BOILED-egg ligand predictive model, it signifies the expected permeability values for both the BBB and the CNS, as well as other predicted properties (metabolic and excretion) imply that all of the examined compounds (Table 8) have good therapeutic potential inhibitors. All the compounds with the exception of the standard drug had a favorable physiochemical profile because their expected values were within the limit. Furthermore, the exact predictive model (BOILED-Egg), which is highly useful in the context of drug discovery and medicinal chemistry and is based on the calculation of lipophilicity given by the logarithm of the partition coefficient between n-octanol and water (Log PO/W) and polarity signaled by the topological polar surface area (TPSA) of small molecules, clearly shows that the Eldepryl molecule (the reference compound) is the only compound that falls out of the blood–brain barrier; as such, the three ligands (13, 31, and 33) pass through the BBB. As a result, the three active ligands outperform the reference drug, and they can be tested in vivo and in vitro.
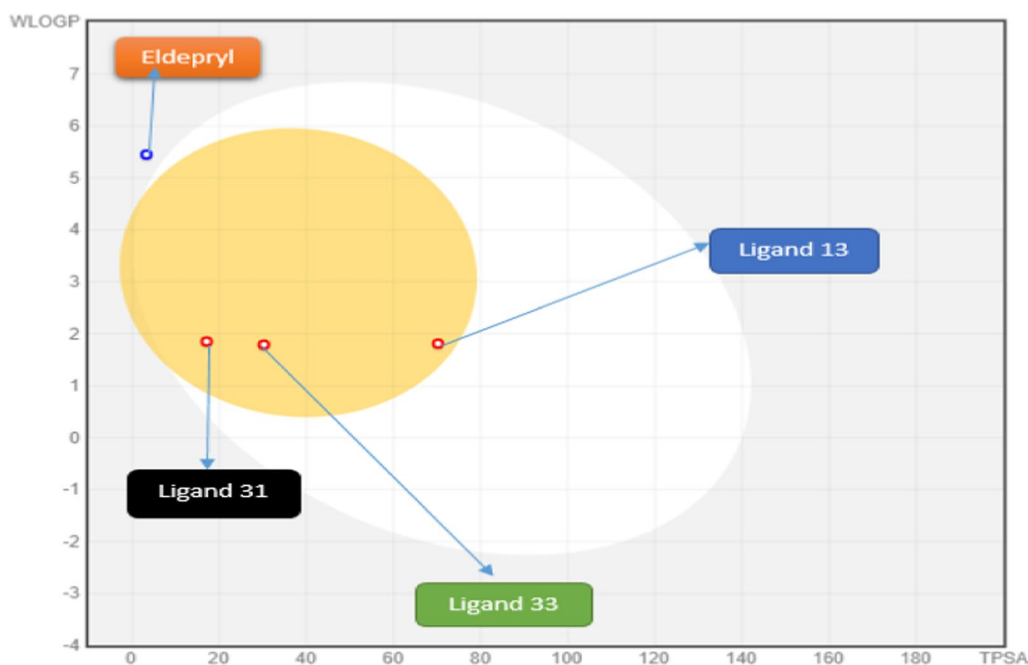

Fig. 11 Model of the most predictive active ligand called BOILED-egg. Molecules 13 (blue), 31 (black), and 33 (green) all fall in the blood–brain barrier. The reference drug (orange) neither falls in the yolk nor albumen

Conclusion

The 37 MAO-B compounds were screened using the aforementioned methods and yielded a model with the following molecular properties: AATS1v, AATS3v, GATS4m, and GATS6e. Good statistical values were $R^2_{\text{train}} = 0.69$, $R^2_{\text{adj}} = 0.63$ $R^2_{\text{pred}} = 0.57$, LOF $= 0.23$, and RMSE $= 0.38$. The model was validated using an evaluation set that confirmed its robustness and could predict the anti-Alzheimer properties of the three selected compounds (13, 31, and 33). A molecular docking study shows the best three compounds (13, 31, and 33) with the lowest binding scores ($- 30.51$ kcal mol^{-1}, $- 31.85$ kcal mol^{-1}, and $- 33.70$ kcal mol^{-1}, respectively) formed the three most stable complexes after binding to the receptor. The docking was validated by re-docking of the co-crystallized compound and getting an RMSD value of 1.7453. Furthermore, the three compounds bind with the active site of the target with the following residues, and this shows two prominent interactions that are hydrogen and hydrophobic with TYR 435, CYS 397, CYS 172, PHE 343, TYR 398, and LYS 296 amino acid residues of the target receptor. Additionally, ADMET/pharmacokinetics evaluation predictions were investigated on these active (three) compounds, and they are orally bioavailable; as such they have therapeutic potential as drugs for the treatment of AD after *in vivo* and *in vitro* analysis.

Declarations

Ethics approval and consent to participate
Not applicable.

Consent for publication
Not applicable.

Competing interests
The authors declare that they have no competing interests.

References

1. Lamptey RN, Chaulagain B, Trivedi R, Gothwal A, Layek B, Singh J (2022) A review of the common neurodegenerative disorders: current therapeutic approaches and the potential role of nanotherapeutics. Int J Mol Sci 23(3):1851
2. Musella A, Gentile A, Rizzo FR, De Vito F, Fresegna D, Bullitta S, Mandolesi G (2018) Interplay between age and neuroinflammation in multiple sclerosis: effects on motor and cognitive functions. Front Aging Neurosci 10:238
3. Creed RB, Menalled L, Casey B, Dave KD, Janssens HB, Veinbergs I, Goldberg MS (2019) Basal and evoked neurotransmitter levels in Parkin, DJ-1, PINK1 and LRRK2 knockout rat striatum. Neuroscience 409:169–179
4. Ayaz M, Ullah F, Sadiq A, Kim MO, Ali T (2019) Natural products-based drugs: potential therapeutics against Alzheimer's disease and other neurological disorders. Front Pharmacol 10:1417
5. Behl T, Kaur D, Sehgal A, Singh S, Sharma N, Zengin G, Bumbu AG (2021) Role of monoamine oxidase activity in Alzheimer's disease: an insight into the therapeutic potential of inhibitors. Molecules 26(12):3724
6. Hung SY, Fu WM (2017) Drug candidates in clinical trials for Alzheimer's disease. J Biomed Sci 24(1):1–12
7. Marucci G, Buccioni M, Dal Ben D, Lambertucci C, Volpini R, Amenta F (2021) Efficacy of acetylcholinesterase inhibitors in Alzheimer's disease. Neuropharmacology 190:108352
8. Behl T, Kaur G, Bungau S, Jhanji R, Kumar A, Mehta V, Fratila O (2020) Distinctive evidence involved in the role of endocannabinoid signalling in Parkinson's disease: a perspective on associated therapeutic interventions. Int J Mol Sci 21(17):6235
9. Zhang L, Song J, Kong L, Yuan T, Li W, Zhang W, Du G (2020) The strategies and techniques of drug discovery from natural products. Pharmacol Ther 216:107686
10. Sharma K (2019) Cholinesterase inhibitors as Alzheimer's therapeutics. Mol Med Rep 20(2):1479–1487
11. Thoe ES, Fauzi A, Tang YQ, Chamyuang S, Chia AYY (2021) A review on advances of treatment modalities for Alzheimer's disease. Life Sci 276:119129
12. Deb PK, Chandrasekaran B, Mailavaram R, Tekade RK, Jaber AMY (2019) Molecular modeling approaches for the discovery of adenosine A2B receptor antagonists: current status and future perspectives. Drug Discov Today 24(9):1854–1864
13. Simoben CV, Ghazy E, Zeyen P, Darwish S, Schmidt M, Romier C, Sippl W (2021) Binding free energy (BFE) calculations and quantitative structure–activity relationship (QSAR) analysis of *Schistosoma mansoni* histone deacetylase 8 (smHDAC8) inhibitors. Molecules 26(9):2584
14. Bekono BD, Ntie-Kang F, Owono Owono LC, Megnassan E (2018) Targeting cysteine proteases from *Plasmodium falciparum*: a general overview, rational drug design and computational approaches for drug discovery. Curr Drug Targets 19(5):501–526
15. D'Ascenzio M, Carradori S, Secci D, Mannina L, Sobolev AP, De Monte C, Ortuso F (2014) Identification of the stereochemical requirements in the 4-aryl-2-cycloalkylidenhydrazinylthiazole scaffold for the design of selective human monoamine oxidase B inhibitors. Bioorg Med Chem 22(10):2887–2895
16. Takao K, Takemura Y, Nagai J, Kamauchi H, Hoshi K, Mabashi R, Sugita Y (2021) Synthesis and biological evaluation of 3-styrylchromone derivatives as selective monoamine oxidase B inhibitors. Bioorg Med Chem 42:116255
17. Banegas-Luna AJ, Cerón-Carrasco JP, Pérez-Sánchez H (2018) A review of ligand-based virtual screening web tools and screening algorithms in large molecular databases in the age of big data. Future Med Chem 10(22):2641–2658
18. Stokes JM, Yang K, Swanson K, Jin W, Cubillos-Ruiz A, Donghia NM, Collins JJ (2020) A deep learning approach to antibiotic discovery. Cell 180(4):688–702
19. Chirico N, Sangion A, Gramatica P, Bertato L, Casartelli I, Papa E (2021) QSARINS-Chem standalone version: a new platform-independent software to profile chemicals for physico-chemical properties, fate, and toxicity. J Comput Chem 42(20):1452–1460

20. Roy K, Ambure P, Kar S, Ojha PK (2018) Is it possible to improve the quality of predictions from an "intelligent" use of multiple QSAR/QSPR/QSTR models? J Chemom 32(4):e2992
21. Khamouli S, Belaidi S, Belaidi H, Belkhiri L (2018) QSAR studies of aminopyrimidine derivatives as *Mycobacterium tuberculosis* protein kinase B inhibitors. Turk Comput Theor Chem 2(2):16–27
22. Chabon JJ, Hamilton EG, Kurtz DM, Esfahani MS, Moding EJ, Stehr H, Diehn M (2020) Integrating genomic features for non-invasive early lung cancer detection. Nature 580(7802):245–251
23. Liu Y, Cheng Z, Liu S, Tan Y, Yuan T, Yu X, Shen Z (2020) Quantitative structure activity relationship (QSAR) modelling of the degradability rate constant of volatile organic compounds (VOCs) by OH radicals in atmosphere. Sci Total Environ 729:138871
24. Yang ZF, Xiao R, Xiong GL, Lin QL, Liang Y, Zeng WB, Cao DS (2022) A novel multi-layer prediction approach for sweetness evaluation based on systematic machine learning modeling. Food Chem 372:131249
25. Stitou M, Toufik H, Bouachrine M, Lamchouri F (2021) Quantitative structure–activity relationships analysis, homology modeling, docking and molecular dynamics studies of triterpenoid saponins as Kirsten rat sarcoma inhibitors. J Biomol Struct Dyn 39(1):152–170
26. Olasupo SB, Uzairu A, Shallangwa GA, Uba S (2020) Chemoinformatic studies on some inhibitors of dopamine transporter and the receptor targeting schizophrenia for developing novel antipsychotic agents. Heliyon 6(7):e04464
27. Ugale VG, Bari SB (2016) Identification of potential Gly/NMDA receptor antagonists by cheminformatics approach: a combination of pharmacophore modelling, virtual screening and molecular docking studies. SAR QSAR Environ Res 27(2):125–145
28. Rai H, Barik A, Singh YP, Suresh A, Singh L, Singh G, Nayak UY, Dubey VK, Modi G (2021) Molecular docking, binding mode analysis, molecular dynamics, and prediction of ADMET/toxicity properties of selective potential antiviral agents against SARS-CoV-2 main protease: an effort toward drug repurposing to combat COVID-19. Mol Divers 25(3):1905–1927
29. Adeniji SE, Shallangwa GA, Arthur DE, Abdullahi M, Mahmoud AY, Haruna A (2020) Quantum modelling and molecular docking evaluation of some selected quinoline derivatives as anti-tubercular agents. Heliyon 6(3):e03639
30. Gürsoy O, Smieško M (2017) Searching for bioactive conformations of drug-like ligands with current force fields: how good are we?. J Cheminform 9(1):1–13
31. Zhang Z, Ricci CG, Fan C, Cheng LT, Li B, McCammon JA (2021) Coupling Monte Carlo, variational implicit solvation, and binary level-set for simulations of biomolecular binding. J Chem Theory Comput 17(4):2465–2478
32. Yadava U (2018) Search algorithms and scoring methods in protein-ligand docking. Endocrinol Int J 6(6):359–367
33. Abduljelil A, Uzairu A, Shallangwa GA, Abechi SE (2022) Structure-based drug design of novel piperazine containing hydrazone derivatives as potent Alzheimer inhibitors: molecular docking and drug kinetics evaluation. Brain Disord 7:100041
34. Ajala A, Uzairu A, Shallangwa G, Abechi S (2022) In-silico design, molecular docking and pharmacokinetics studies of some tacrine derivatives as anti-Alzheimer agents: theoretical investigation. Adv J Chem Sect A 5(1):59–69
35. Khan T, Dixit S, Ahmad R, Raza S, Azad I, Joshi S, Khan AR (2017) Molecular docking, PASS analysis, bioactivity score prediction, synthesis, characterization and biological activity evaluation of a functionalized 2-butanone thiosemicarbazone ligand and its complexes. J Chem Biol 10(3):91–104
36. Hadda TB, Rastija V, AlMalki F, Titi A, Touzani R, Mabkhot YN, Siddiqui BS (2021) Petra/osiris/molinspiration and molecular docking analyses of 3-hydroxy-indolin-2-one derivatives as potential antiviral agents. Curr Comput Aided Drug Des 17(1):123–133
37. Powers DM (2020) Evaluation: from precision, recall and F-measure to ROC, informedness, markedness and correlation. arXiv preprint arXiv:2010.16061.
38. Brown BP, Mendenhall J, Geanes AR, Meiler J (2021) General purpose structure-based drug discovery neural network score functions with human-interpretable pharmacophore maps. J Chem Inf Model 61(2):603–620
39. Salman M, Nandi S (2017) QSAR and pharmacophore modeling of anti-tubercular 6-Fluoroquinolone compounds utilizing calculated structural descriptors. Med Chem Res 26(9):1903–1914
40. Adeniji SE, Arthur DE, Abdullahi M, Adalumo OB (2020) Computational investigation, virtual docking simulation of 1, 2, 4-Triazole analogues and insillico design of new proposed agents against protein target (3IFZ) binding domain. Bull Natl Res Centre 44(1):1–17
41. Ishola AA, Adedirin O, Joshi T, Chandra S (2021) QSAR modeling and Pharmacoinformatics of SARS coronavirus 3C-like protease inhibitors. Comput Biol Med 134:104483
42. Sanchez-Moreno J, Bonnin CDM, González-Pinto A, Amann BL, Solé B, Balanzá-Martinez V, Varo C (2018) Factors associated with poor functional outcome in bipolar disorder: sociodemographic, clinical, and neurocognitive variables. Acta Psychiatr Scand 138(2):145–154
43. Popovic S, Arifi F, Bjelica D (2017) Standing height and its estimation utilizing foot length measurements in Kosovan adults: national survey. Int J Appl Exerc Physiol 6(2):1–7
44. Huang H, Cheng Y, Weibel R (2019) Transport mode detection based on mobile phone network data: a systematic review. Transport Res Part C Emerg Technol 101:297–312
45. Bacho M, Coelho-Cerqueira E, Follmer C, Mohammad Nabavi S, Rastrelli L, Uriarte E, Sobarzo-Sanchez E (2017) A medical approach to the monoamine oxidase inhibition by using 7Hbenzo [e] perimidin-7-one derivatives. Curr Top Med Chem 17(4):489–497
46. Dhiman P, Malik N, Khatkar A (2017) Docking-related survey on natural-product-based new monoamine oxidase inhibitors and their therapeutic potential. Combin Chem High Throughput Screen 20(6):474–491
47. Nguyen NT, Nguyen TH, Pham TNH, Huy NT, Bay MV, Pham MQ, Nam PC, Vu VV, Ngo ST (2020) Autodock Vina Adopts More Accurate Binding Poses but Autodock4 Forms Better Binding Affinity. J Chem Inf Model 60(1):204–211
48. Catalano R, Procopio F, Chavarria D, Benfeito S, Alcaro S, Borges F, Ortuso F (2022) Molecular modeling and experimental evaluation of non-chiral components of bergamot essential oil with inhibitory activity against human monoamine oxidases. Molecules 27(8):2467
49. Sood D, Kumar N, Singh A, Sakharkar MK, Tomar V, Chandra R (2018) Antibacterial and pharmacological evaluation of fluoroquinolones: a chemoinformatics approach. Genom Inform 16(3):44
50. Lam PCH, Abagyan R, Totrov M (2019) Macrocycle modeling in ICM: benchmarking and evaluation in D3R Grand Challenge 4. J Comput Aided Mol Des 33(12):1057–1069

Publisher's Note